

Wavelet Regularized Alternating Minimization Algorithm for Low Dose X-ray CT

Jingwei Lu*, Joseph A. O'Sullivan*, *Fellow, IEEE*, and David G. Polite†, *Member, IEEE*

*Department of Electrical and Systems Engineering, Washington University in St. Louis, St. Louis, MO 63130

†Mallinckrodt Institute of Radiology, Washington University School of Medicine, St. Louis, MO 63110

Abstract—X-ray computed tomography reconstruction has evolved over 40 years for medical, security, and industrial applications. Compared to traditional analytic reconstruction techniques such as filtered back projection (FBP), statistical reconstruction algorithms like alternating minimization (AM) provide improved image quality and can incorporate prior information. Increasing patient safety through reduced radiation dose results in fewer measured photons. Penalized AM is a powerful tool for maintaining image quality with less data, but the weight of penalty must be chosen carefully. If the penalty weight is too low, noise may not be suppressed and artifacts may be exhibited, such as those due to sharp discontinuities in attenuation at edges of dense material. If the penalty weight is higher, noise and artifacts may be reduced, but at the expense of introducing bias into the reconstruction. These contradicting requirements for the weight of the penalty limit our ability to improve reconstructed image quality in a low dose scenario. In this paper, we develop a new algorithm called wavelet regularized alternating minimization (wav-AM) by introducing a second penalty term on wavelet coefficients. By solving this dual domain optimization problem, we are able to perform 3D reconstruction of scanned baggage with low X-ray photon intensity. A medical imaging application of the wav-AM algorithm will be provided to illustrate the performance in image quality improvement. Evaluation of these real data reconstructions show reduced noise and artifacts without biasing the estimated attenuation of objects of known attenuation. The wav-AM algorithm features guaranteed convergence and increases the computational burden compared to the usual penalized AM algorithm only negligibly, even though we are solving a dual domain optimization problem.

Index Terms—Computed Tomography, Low Dose, Wavelet, Alternating Minimization, Dual Domain Optimization

I. SUMMARY

X-ray CT image reconstruction is often viewed as a regularized optimization problem in which we try to minimize a cost function with two terms. The first term is a data fitting term, such as squared error, weighted least-squares error [1], or I-divergence [2]. The second term is a penalty that contains prior information about the image, and usually promotes smoothness in the reconstructed image. Typical choices of penalty terms are total variation or a Huber-type penalty [3][4]. The balance between the data fitting term and the penalty term is controlled by the choice of the penalty weight. A low weight for the penalty retains details in the image but does not suppress noise or artifacts. A higher penalty weight reduces noise and artifacts, but the trade-off is possible loss of detail due to a less accurate fitting of the forward projected image to the measured data. So, in low dose CT, choosing a good penalty weight is not

only crucial but also difficult. The contradicting requirements favoring a low weight to optimize some image characteristics and a high weight to optimize other image characteristics make it difficult to find an optimal penalty weight. To solve this problem, we introduce a new iterative algorithm called wavelet regularized alternating minimization (wav-AM), which has the following properties:

- In addition to the usual neighborhood smoothness penalty, an extra penalty term is introduced on wavelet coefficients of the reconstructed image.
- Instead of optimizing this augmented cost function in the image domain alone, we view it as a dual optimization problem on the image domain and the wavelet coefficient domain.
- By solving this dual domain optimization problem, we are able to reduce artifacts and still retain an unbiased reconstruction.
- The wav-AM algorithm retains the convergence properties of the usual penalized AM algorithm.
- Compared with the usual penalized AM algorithm, the introduction of the wavelet penalty does not increase the computational cost significantly. Furthermore, other acceleration methods can be applied.

II. INTRODUCTION

The AM algorithm is one of the most efficient X-ray CT reconstruction methods [2]. The data fitting term in (1) is I-divergence between data y and the estimated mean q . In [2] it is shown that minimizing I-divergence is equivalent to maximizing Poisson log-likelihood. We formulate our estimation problem as

$$\begin{aligned} u &= \arg \min_u \sum_i I(y_i || q_i(u)) \\ &= \arg \min_u \sum_i [y_i \log \frac{y_i}{q_i(u)} - y_i + q_i(u)], \end{aligned} \quad (1)$$

where $q_i(u) = I_i \exp[-\sum_j h_{ij} u_j]$, $u \in R_+^N$ is the image we want to reconstruct, I_i is the mean air scan photon counts at source-detector pair i , and h_{ij} is an element in the system matrix that represents the contribution of voxel j to source-detector pair i .

If we add a penalty term to (1), the resulting penalized maximum-likelihood estimate is

$$\min_u F(u) = \sum_i I(y_i || q_i(u)) + \lambda R(u), \quad (2)$$

where $R(u)$ is a penalty term used to enforce smoothness on the image. Here we choose a Huber-type edge preserving penalty which has the following form [3][5]

$$R(u) = \sum_j \sum_{k \in N_j} w_{jk} \phi(u_j - u_k), \quad (3)$$

where

$$\phi(u_j - u_k) = \frac{1}{\delta^2} (|\delta(u_j - u_k)| - \log(1 + |\delta(u_j - u_k)|)). \quad (4)$$

When $u_j - u_k$ is small, ϕ performs like a quadratic function, when $u_j - u_k$ is large, ϕ performs like a linear function and in this way we achieve the edge preserving effect. Another advantage of this choice is that we have continuous first order and second order derivatives at the point 0. Parameter δ is set to be 1000 in this paper, N_j is the set of neighboring voxels around voxel j . The weights w_{jk} control the relative contribution of every neighboring voxel to voxel j . Here, we choose a 26-voxel neighborhood and their weights are taken as the normalized inverse distance to voxel j .

Due to the existence of the penalty term, we do not have a closed form solution to problem (2). Instead, we decouple the cost function [2] with respect to every element u_j and then use Newton's method which requires the first order and second order derivative of the cost function. The corresponding derivatives are

$$\frac{\partial F(u_j)}{\partial u_j} = \sum_i h_{ij} y_i - \beta_j \exp\{-Z(u_j - u_j^n)\} + \frac{\partial R(u_j)}{\partial u_j} \quad (5)$$

and

$$\frac{\partial^2 F(u_j)}{\partial u_j^2} = \beta_j Z \exp\{-Z(u_j - u_j^n)\} + \frac{\partial^2 R(u_j)}{\partial u_j^2}, \quad (6)$$

where $\beta_j = \sum_i h_{ij} q_i(u)$, u_j^n is the current estimate and Z is a constant to enforce convergence.

Then we follow the standard Newton's method to update every image voxel by

$$u_j^{n+1} = u_j^n - \left[\frac{\partial F(u_j)}{\partial u_j} \right] / \left[\frac{\partial^2 F(u_j)}{\partial u_j^2} \right], \quad (7)$$

where u_j^n is the reconstructed voxel j at iteration n .

The data package used in this paper was acquired from a SureScan™ x1000 Explosive Detection System which scanned a NIST A phantom [6]. As shown in Fig.1, the object of interest is a Delrin cylinder wrapped with aluminum, copper, tin and lead. In Fig. 2, we plot the histogram of numbers of source-detector pairs for different photon counts. From it we can see that the maximum photon counts at a single pair is less than 2000, and a large portion of pairs have very limited photon counts. The data is photon starved and we use the AM algorithm to deal with this low dose problem.

Reconstruction results from the AM algorithm are shown in Fig. 3, Fig. 4, Fig. 5 and Fig. 6. In Fig. 3, we show the lateral slice 200 reconstruction which shows the geometry of the NIST A phantom. Fig. 3(a), (b), (c) and (d) correspond to results from unpenalized AM algorithm, penalized AM algorithm with $\lambda = 1000$, $\lambda = 3000$ and $\lambda = 15000$. We can identify the bright metal wraps on the edges and the noise level is reduced if we increase the penalty weight λ . In Fig. 4, the

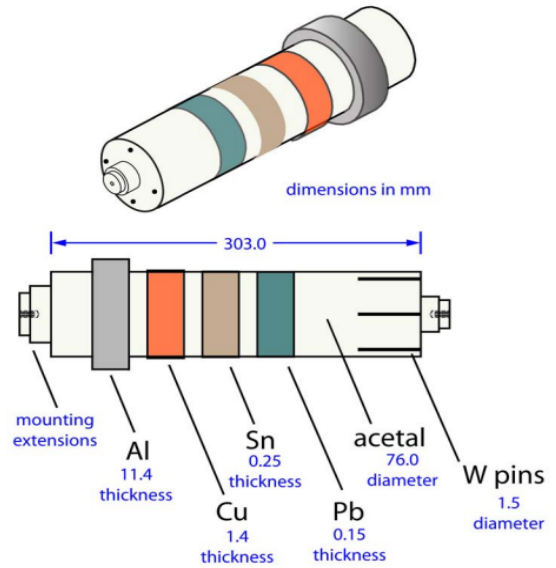


Fig. 1: Geometry of NIST A phantom.

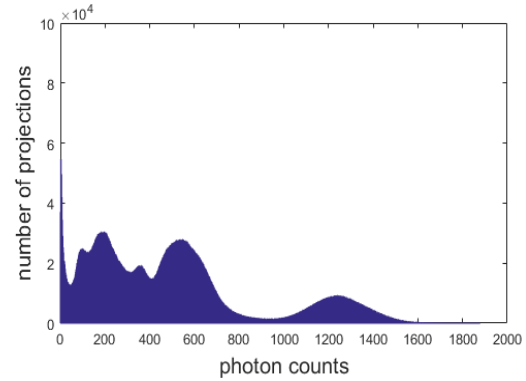


Fig. 2: Histogram of photon counts.

left column shows the reconstructed lateral slice No. 99. In this slice, the object of interest is a Delrin cylinder wrapped with aluminum. From top to bottom, the images are reconstructed with unpenalized AM, penalized AM with $\lambda = 1000$, 3000, and 15000. The right column shows the corresponding profiles of row 186 in slice No. 99 which are highlighted in the left column. In unpenalized AM we get very noisy results and with the increase in penalty weight λ , the noise is reduced and we have smooth images. However, the peak value is dramatically decreased and the value in the center is increased with heavier penalty weights. This direct comparison is shown in Fig. 5. We conclude that a heavy penalty will generate biased results.

In Fig. 6, we use another slice to show the performance of the AM algorithm. Fig. 6 shows reconstructed image slice No. 92 with unpenalized AM, penalized AM with $\lambda=1000$, 3000 and 15000. Slice 92 is on the edge of aluminum wrapped around the Delrin cylinder, and the disk in the figure is pure Delrin. We can see that without a penalty term, as in Fig. 4(a), the image has many streaks coming out tangent to the boundary of the Delrin cylinder and dotted noise is visible across the entire area. When we apply the penalized AM

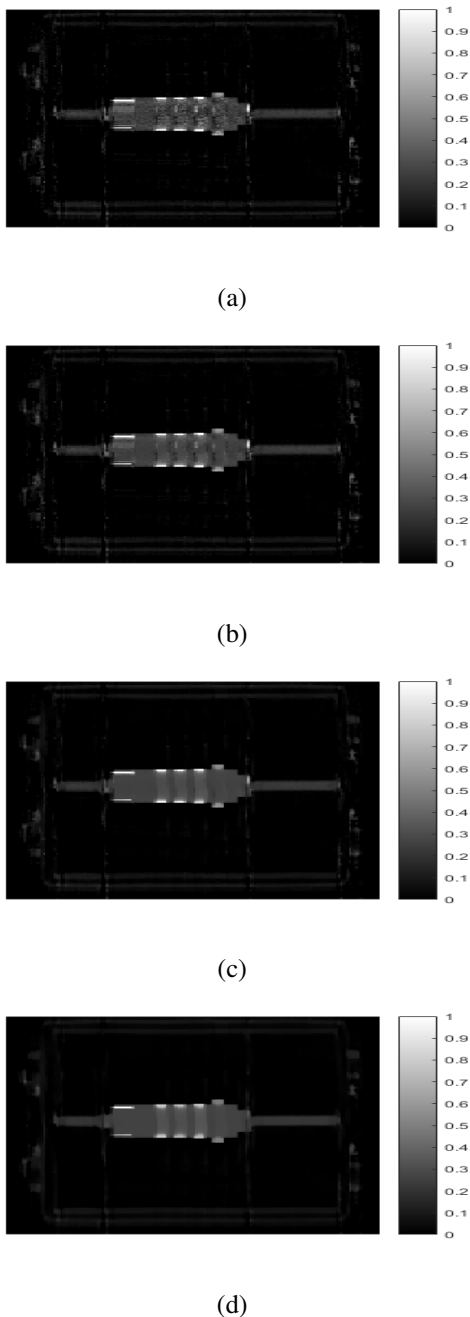


Fig. 3: Sagittal slice No. 200 with (a) unpenalized AM, (b) penalized AM $\lambda = 1000$, (c) penalized AM $\lambda = 3000$, and (d) penalized AM $\lambda = 15000$. The display window is $[0 \ 1]\text{mm}^{-1}$.

algorithm, if the weight is low like $\lambda = 1000$ or $\lambda = 3000$, we still have severe artifacts and noise. We must increase the weight to 15000 to finally suppress these artifacts and noise.

From the results of slices No. 99 and No. 92, we have contradictory requirements in the choice of penalty weights. Low weights are not able to reduce artifacts and noise, and the high weights will generate biased reconstruction.

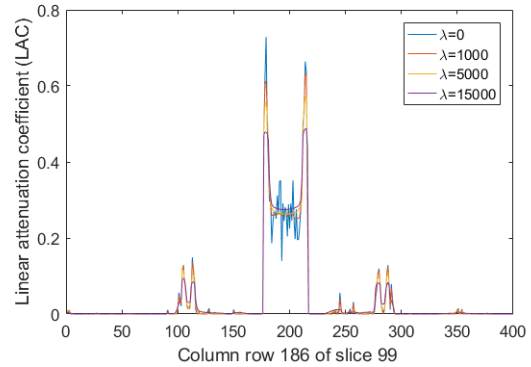


Fig. 5: Profile comparison for different penalty weight λ .

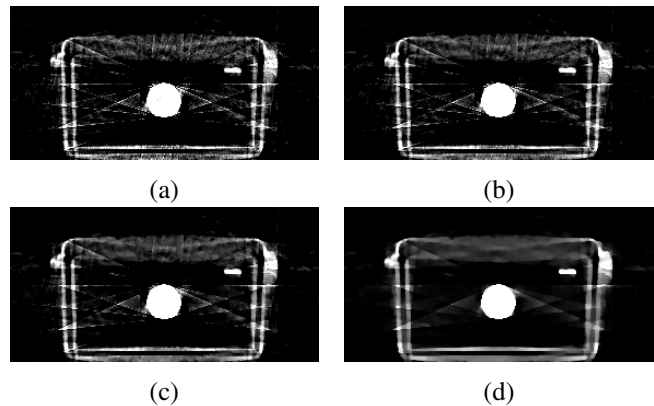


Fig. 6: Reconstructed slice No. 92 (a) unpenalized AM, (b) penalized AM, $\lambda = 1000$, (c) penalized AM, $\lambda = 3000$, (d) penalized AM, $\lambda = 15000$. The display window has been tightened to $[0 \ 0.15]\text{mm}^{-1}$ to deliberately emphasize streaks associated with measurements tangential to circular object.

III. METHOD

To deal with the contradiction we stated in the last section, we add an extra penalty term in the wavelet coefficient domain and our problem is reformulated as

$$\min_u F(u) = \sum_i I(y_i || q_i(u)) + \lambda R(u) + \gamma Q(u), \quad (8)$$

where $Q(x) = \|\Phi x\|_1$ [7], and Φ is an orthogonal wavelet transform operator which transforms image u into its corresponding wavelet $\tilde{u} \in R^N$. Due to the existence of Φ , which leads to dramatic increase in computational cost in Newton's method, it is hard to solve this problem directly on image domain. Here, we use Sparse Reconstruction by Separable Approximation algorithm (SpaRSA) [8]. Since in (8), $I(y_i || q_i(u))$ and $R(u)$ are both convex in u , we can cast the problem in the following form

$$\min_u F(u) = g(u) + \gamma Q(u), \quad (9)$$

where $g(u) = \sum_i I(y_i || q_i(u)) + \lambda R(u)$. Then we generate a sequence of iterates $\{u^n, n = 0, 1, \dots\}$ and tailor our problem

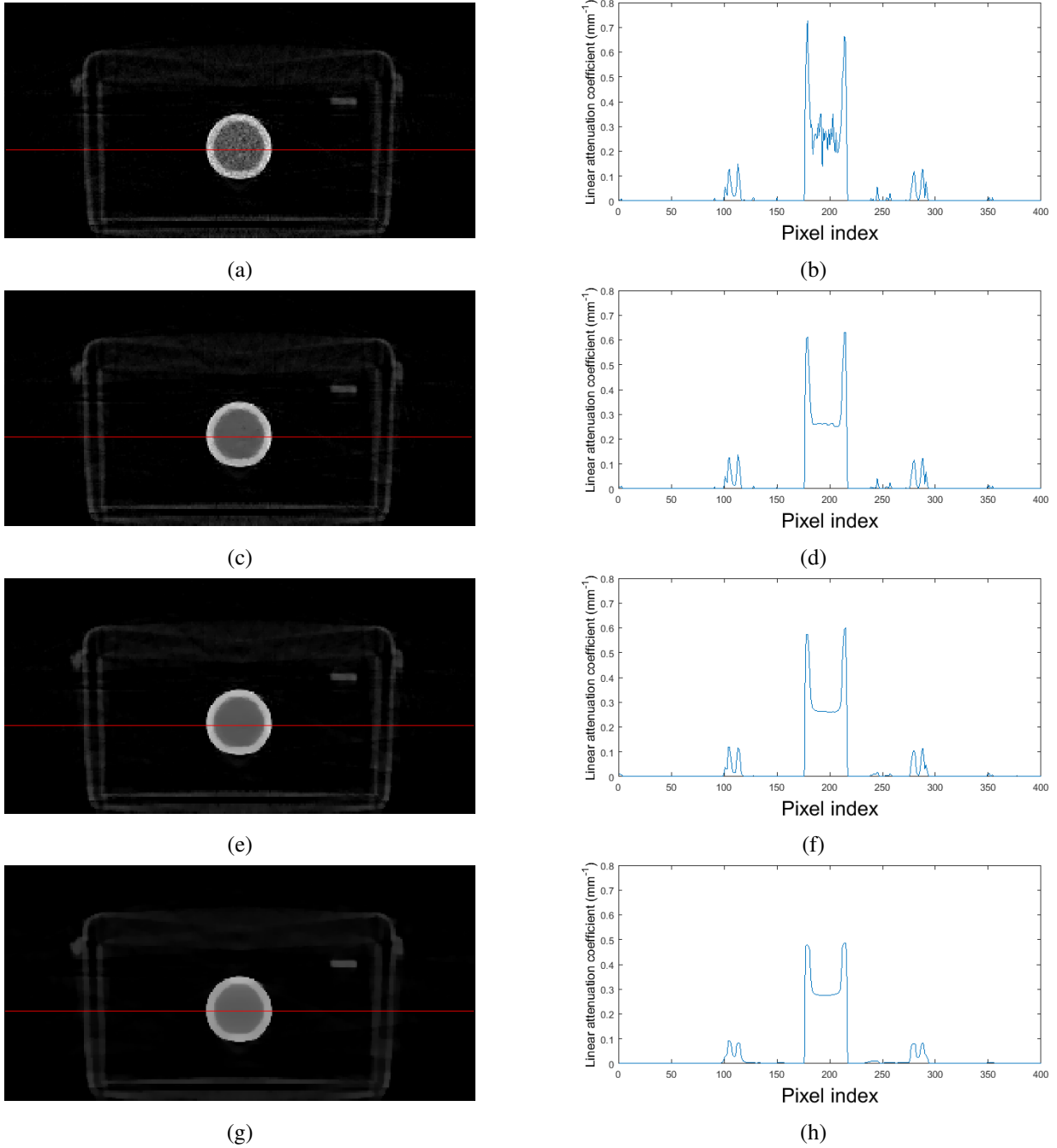


Fig. 4: Lateral slice No. 99 and profile of row 186. (a)(b) unpenalized AM, (c)(d) penalized AM with $\lambda = 1000$, (e)(f) penalized AM with $\lambda = 3000$, (g)(h) penalized AM with $\lambda = 15000$. The display window is $[0 \ 0.8] \text{ mm}^{-1}$.

in which the following sub-problem can be solved efficiently at each iteration

$$u^{n+1} = \arg \min_z (z - u^n) \frac{\partial g(u^n)}{\partial u} + \frac{\alpha_n}{2} \|z - u^n\|_2^2 + \gamma Q(z). \quad (10)$$

for some $\alpha_n \in R^+$. An equivalent form of sub-problem (10) is

$$u^{n+1} = \arg \min_z \frac{1}{2} \|z - \hat{u}^{n+1}\|_2^2 + \frac{\gamma}{\alpha_n} Q(z), \quad (11)$$

where

$$\hat{u}^{n+1} = u^n - \frac{1}{\alpha_n} \frac{\partial g(u^n)}{\partial u}. \quad (12)$$

α_n is taken as the second order derivative of $g(u^n)$ which is given in (6) and $\frac{\partial g(u^n)}{\partial u}$ is exactly function (5). Then we have the following problem,

$$u^{n+1} = \arg \min_z \frac{1}{2} \|z - \hat{u}^{n+1}\|_2^2 + \frac{\gamma}{\alpha_n} \|\Phi z\|_1, \quad (13)$$

where $\hat{u}^{n+1} = u^n - [\frac{\partial g(u^n)}{\partial u}] / [\frac{\partial^2 g(u^n)}{\partial u^2}]$ is the Newton's iteration for problem (2).

Since Φ is an orthogonal wavelet transform operator, (11)

is equivalent to the following minimization problem

$$u^{n+1} = \arg \min_z \frac{1}{2} \|\Phi z - \Phi \hat{u}^{n+1}\|_2^2 + \frac{\gamma}{\alpha_n} \|\Phi z\|_1 \quad (14)$$

or

$$\tilde{u}^{n+1} = \arg \min_{\tilde{z}} \frac{1}{2} \|\tilde{z} - \tilde{\hat{u}}^{n+1}\|_2^2 + \frac{\gamma}{\alpha_n} \|\tilde{z}\|_1, \quad (15)$$

where \tilde{z} , $\tilde{\hat{u}}$ represent the wavelet coefficients of z and \hat{u} , respectively. It has been demonstrated that the iterative shrinkage thresholding algorithm (ISTA) [9] solves this problem by

$$\tilde{u}^{n+1} = (|\tilde{\hat{u}}^{n+1}| - \frac{\gamma}{\alpha_n})_+ \text{sgn}(\tilde{\hat{u}}^{n+1}). \quad (16)$$

In this way, we solve problem (8) in a two-step update scheme: first solve a traditional penalized AM problem in the image domain, and then in the wavelet domain update the corresponding wavelet coefficients based on (16).

The pseudo-code for wav-AM is shown below.

Algorithm 1 wavelet regularized alternating minimization

Initialize u

for $n = 1$ to N **do**

A. Solve traditional penalized AM by Newton's method

1. Set $m = 0$, and $u_{j_Newton}^{(m=0)} = u_j^{(n)}$;
2. $u_{j_Newton}^{(m+1)} = u_{j_Newton}^{(m)} - [\frac{\partial g(u^n)}{\partial u}] / [\frac{\partial^2 g(u^n)}{\partial u^2}]$
3. Iterate until convergence, $\tilde{u}_j^{n+1} = \Phi u_{j_Newton}^{(m+1)}$

B. Update \tilde{u}_j by (16)

1. $\tilde{u}^{n+1} = (|\tilde{\hat{u}}^{n+1}| - \frac{\gamma}{\alpha_n})_+ \text{sgn}(\tilde{\hat{u}}^{n+1})$
2. $u^{n+1} = \Phi^{-1} \tilde{u}^{n+1}$

end for

IV. EXPERIMENT RESULTS

A. NIST A Phantom

We use the same sample bag data to illustrate the performance of wav-AM. The orthogonal wavelet is chosen to be a Daubechies D4 wavelet. The parameters λ and γ are both equal to 1000. In Fig. 7(a), the lateral slice No. 99 is shown. In Fig. 7(b), the profile of the AM algorithm with different penalty weights λ and the wav-AM algorithm is shown, the wav-AM will generate unbiased results compared with high penalty weights and produce smoother image compared with small penalty weights. In Fig. 7(c), the peak values profiles are shown. We find that adding an extra wavelet penalty does not shift the peak values and they align well with the results from the AM algorithm with $\lambda = 1000$. In Fig. 7(d), we plot the profile of the cross section of Delrin. Compared with results from the AM algorithm with $\lambda = 1000$, the wav-AM reconstruction has a even smoother Delrin reconstruction and retain the sharp edge from air to aluminum and from aluminum to Delrin.

In Fig. 8, the reconstructed slice No. 92 from wav-AM is shown. Compared with the traditional AM algorithm, the wav-AM algorithm is able to dramatically reduce the streak artifacts and dotted noise with relatively low λ . We avoid using a huge weight like $\lambda = 15000$ and our reconstruction is unbiased, smooth and also artifact-reduced.

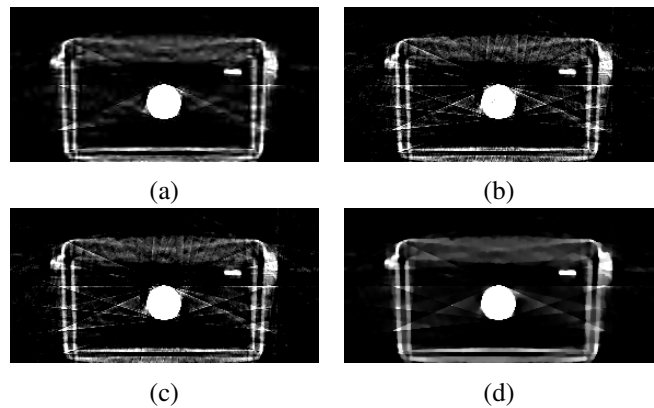


Fig. 8: Slice No. 92 (a) wav-AM with $\lambda = 1000$, $\gamma = 1000$, (b) unpenalized AM, (c) penalized AM with $\lambda = 1000$, (d) penalized AM with $\lambda = 15000$. The display window has been tightened to $[0 \ 0.15] \text{ mm}^{-1}$ to deliberately emphasize streaks.

Since we avoid computing the wavelet transform operator Φ directly in the Newton's step, compared with the traditional AM algorithm, the extra computational cost in wav-AM is due to the wavelet thresholding step, and this step is very fast in the Matlab environment. The total increase in computation time is less than 5%.

B. Patient Data

The patient data was collected from Philips Brilliance Big Bore scanner with 816 detectors per detector row, 1320 source positions per rotation and collimation 16 by 1.5mm. The data has two energy measurements: 90kVp (375mAs) and 140kVp (295mAs). In this section, we select 140kVp measurement as our data input. The image size is 610×610 with pixel size $1\text{mm} \times 1\text{mm}$.

In Fig. 9(a), we use the standard FBP method to reconstruct the image and from it we can see a lot of noise and streaks across the body. In Fig. 9(b), we use the penalized AM algorithm with $\lambda = 10^6$. The noise is reduced and we can see clear anatomical structure inside the body, however the streaking artifacts are still prominent. In Fig. 9(c), we increase the penalty weight λ to 5×10^6 , and the streaks inside the body are suppressed, however the streaks on the left and right edges are still prominent. Another problem is that $\lambda = 5 \times 10^6$ is too large and we have oversmoothed images. In Fig. 9(d), we use the wav-AM algorithm with $\lambda = 10^6$ and $\gamma = 2 \times 10^5$. We reduce the noise and streaking artifacts simultaneously without sacrificing the resolution. In this experiment, the parameter δ is set to be 5000 in both the penalized AM algorithm and the wav-AM algorithm.

V. CONCLUSIONS

An iterative algorithm for low dose X-ray CT image reconstruction is formulated and presented by the wav-AM framework. The algorithm is able to suppress artifacts and heavy noise brought by low penalty weights and unbiased reconstruction generated with high penalty weights in the traditional penalized AM framework. Our two-step update

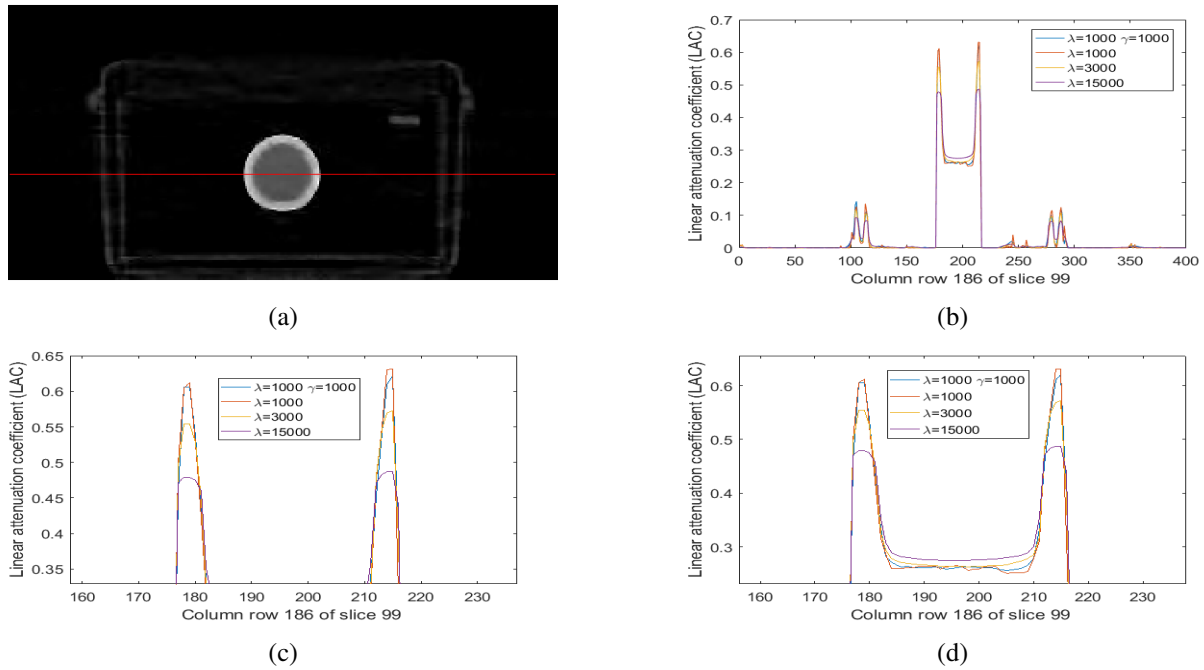


Fig. 7: (a) is slice No. 99 and (b) is the profile comparison of column 86. The display window is $[0 \ 0.8] \text{ mm}^{-1}$. (c) and (d) are detailed profiles of aluminum and Delrin, respectively.

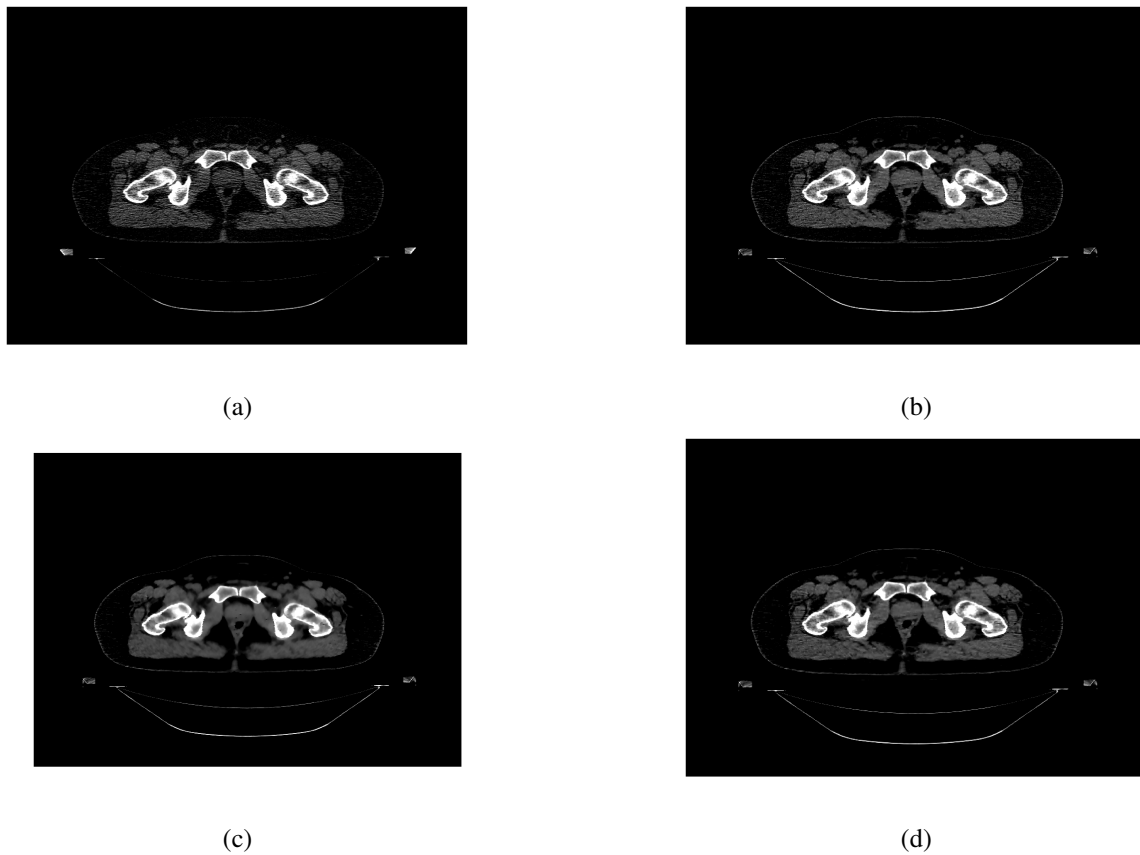


Fig. 9: Patient data reconstructions: (a) the standard FBP method, (b) the penalized AM algorithm with $\lambda = 10^6$, (c) the penalized AM algorithm with $\lambda = 5 \times 10^6$, and (d) the wav-AM algorithm with $\lambda = 10^6$ and $\gamma = 2 \times 10^5$. The display window is $[0.016, 0.024] \text{ mm}^{-1}$.

scheme provides an efficient dual domain method to solve this dual penalty problem without sacrificing speed and do not require extra computation resource. The extra penalty gives us another level of flexibility to improve image quality which is promising for further research. And in terms of application, acceleration methods used with the AM algorithm like ordered subsets [10] can be applied directly.

VI. ACKNOWLEDGMENTS

We thank Carl Bosch, Nawfel Tricha, Sean Corrigan, Michael Hollenbeck, and Assaf Mesika of SureScan™ Corporation for their contribution to the collection, formatting, and sharing of the data.

REFERENCE

- [1] Q. Xu, D. Yang, J. Tan, A. Sawatzky, and M. A. Anastasio, "Accelerated fast iterative shrinkage thresholding algorithms for sparsity-regularized cone-beam CT image reconstruction," *Medical Physics*, vol. 43, p. 1849, Apr. 2016.
- [2] J. A. O'Sullivan, D. L. Snyder, and B. R. Whiting, "Alternating minimization algorithms for transmission tomography using energy detectors," in *Proc. Conf. Record of the Thirty-Sixth Asilomar Conf. Signals, Systems and Computers*, vol. 1, pp. 144–147, vol.1, Nov. 2002.
- [3] J. A. Fessler, E. P. Ficaro, N. H. Clinthorne, and K. Lange, "Grouped-coordinate ascent algorithms for penalized-likelihood transmission image reconstruction," *IEEE Transactions on Medical Imaging*, vol. 16, no. 2, pp. 166–175, 1997.
- [4] L. I. Rudin and S. Osher, "Total variation based image restoration with free local constraints," in *Proc. 1st Int. Conf. Image Processing*, vol. 1, pp. 31–35, vol.1, Nov. 1994.
- [5] K. Lange, R. Carson, *et al.*, "EM reconstruction algorithms for emission and transmission tomography," *J Comput Assist Tomogr*, vol. 8, no. 2, pp. 306–16, 1984.
- [6] "American national standard for evaluating the image quality of x-ray computed tomography (CT) security-screening systems," *ANSI N42.45-2011*, pp. 1–58, May 2011.
- [7] S. Degirmenci, D. G. Polite, C. Bosch, N. Tricha, and J. A. O'Sullivan, "Acceleration of iterative image reconstruction for x-ray imaging for security applications," in *SPIE/IS&T Electronic Imaging*, pp. 94010C–94010C, International Society for Optics and Photonics, 2015.
- [8] S. J. Wright, R. D. Nowak, and M. A. T. Figueiredo, "Sparse reconstruction by separable approximation," *IEEE Transactions on Signal Processing*, vol. 57, pp. 2479–2493, July 2009.
- [9] A. Beck and M. Teboulle, "A fast iterative shrinkage-thresholding algorithm for linear inverse problems," *SIAM Journal on Imaging Sciences*, vol. 2, no. 1, pp. 183–202, 2009.
- [10] H. Erdogan and J. A. Fessler, "Ordered subsets algorithms for transmission tomography," *Physics in Medicine and Biology*, vol. 44, pp. 2835–2851, Nov. 1999.